

MODEL TESTS ON SAND BOILING AROUND COFFERDAM CONSIDERING THE EFFECT OF GEOMATERIAL PROPERTIES

*Tatsuya Matsuda¹, Naoto Naito¹ and Kinya Miura¹

¹Department of Architecture and Civil Engineering, Toyohashi University of Technology, Japan

*Corresponding Author, Received: 15 June 2022, Revised: 29 Dec. 2022, Accepted: 28 Jan. 2023

ABSTRACT: Cofferdams are widely employed for constructing structures in rivers and under groundwater tables. However, cofferdams constructed with sheet piles sometimes destabilize owing to sand boiling due to excessive upward seepage force inside cofferdams near the sheet piles. Therefore, a rational design method for cofferdams is indispensable for ensuring the reliability of the structures resting on the integrated foundation ground, even in water. Particularly the integrity of the foundation ground inside the cofferdam is examined by assessing the balance between the weight of the ground material and the upward seepage force, where the mechanical properties of the ground material or the scale effect of soil particles need to be sufficiently considered. In this study, we conducted a series of model tests on sand boiling occurrence inside a cofferdam. Two cofferdam models of different sizes were prepared, and several ground materials with different grain-size distributions and relative densities were employed. We analyzed the seepage flow process until sand boiling in every model test and determined the seepage flow condition for sand boiling and ground formation after failure. Consequently, we determined the perceptible effects of the mechanical properties of the ground material and the scale of the model cofferdam on the critical seepage condition for sand boiling failure.

Keywords: Cofferdams, Seepage failure, Scaling model test, Scale effect

1. INTRODUCTION

Cofferdams have been widely employed to develop structural foundations in rivers and groundwater tables. They are constructed with sheet piles; however, sometimes, they are damaged owing to sand boiling. Moreover, the ground inside the cofferdams is disintegrated, causing an upward seepage force inside the cofferdams around the sheet piles. In addition, the disintegration of the ground inside the cofferdam reduces its load-bearing capacity for structures.

Several researchers have investigated the stability of cofferdams concerning the seepage force and associated sand boiling. The primary design of a cofferdam constructed with sheet piles was conducted following the method proposed by Terzaghi and Peck (1948) [1]. In particular, in the study, the critical hydraulic head difference between the outside and inside of the cofferdam, triggering the sand boiling occurrence, was estimated following a two-dimensional static seepage analysis, where the cofferdam was implicitly modeled as a strip-shaped structure. In the implemented method, the mechanical properties of the ground material, except its density, were not considered when calculating the critical hydraulic head difference.

Miura et al. (1999 [2], 2001 [3]) studied cases where cofferdams were severely damaged due to sand boiling when constructing bridge piers in rivers. The authors conducted a series of three-

dimensional seepage analyses using the finite element method (FEM). As a result, the authors determined that the seepage force largely depended on the plane shape of the cofferdam and that of the vertical section; the critical hydraulic head difference for rectangular and round-shaped cofferdams was approximately two-thirds of that for strip-shaped cofferdam.

Tanaka and Verruijt (1999) [4] performed simulations on a medium-dense sand ground under two-dimensional conditions to investigate the seepage failure of the ground behind sheet piles and the mechanism of local seepage failure. The results of the model tests showed that the prismatic failure concept effectively evaluated the critical hydraulic head difference for the sand boiling occurrence, where a certain soil prism loses equilibrium. They also clarified that the hydraulic head difference for the prismatic sand model was approximately 10 % freeboard in between compared to that for a total failure.

Asaoka and Kodaka (1992) [5] classified saturated soil failure problems into four types. Type I: The failure of loose and/or normally consolidated soils under fully drained loading conditions. Type II: The same soils as Type I but under perfectly undrained conditions. Type III: The failure of dense and/or overconsolidated soils under fully drained conditions. Type IV: The same soils as Type III but under perfectly undrained conditions. Based on this classification, the authors conducted various model tests to analyze the failure problem due to seepage

and soil-water coupled limit equilibrium, combined with the critical state concept. Their findings regarding the relationship between the failure load and the failure mode can be summarized as follows: (1) the smallest failure load in loose sand occurred under undrained conditions, (2) the largest failure load with the largest failure region occurred in dense sand under undrained conditions, and (3) no global deformation was observed before failure within the soil under fully drained condition, suggesting the development of very localized shear deformation in the sand.

Benmebarek et al. (2005) [6] used the FLAC-2D code to analyze the seepage failure of sandy soil in a cofferdam subjected to upward seepage flow. The results indicated that the soil dilation angle significantly affected the shape of the failure mechanism. In particular, for a dilating material, the failure occurred as a triangular prism due to heaving. In contrast, in other cases, the failure occurred as a rectangular prism, and the obtained widths of the rectangular prisms were smaller than those obtained by Terzaghi's method (Terzaghi and Peck, 1948).

Okajima et al. (2009) [7] performed simulations designed to study the seepage failure of soil behind fixed sheet piles. In particular, an elasto-plastic finite element (FE) model was implemented to verify its effectiveness. Model tests and FE analyses were conducted for different relative densities of the ground. Terzaghi's method was also investigated using test data. The results confirmed the effectiveness of Terzaghi's method for calculating failure head differences in the loose-density ground. Moreover, the results showed that in densely dense soils, the shape of the soil differed from the rectangular shape assumed by Terzaghi.

Numerical methods have been developed to reproduce seepage failure with large-scale ground deformation. For instance, Maeda and Sakai (1994) [8] developed the smoothed particle hydrodynamics (SPH) method, a discrete and continuous analysis considering the three phases of soil, water, and air interactions. The seepage failure around sheet piles and river embankments was successfully simulated. Moreover, Maeda and Sakai (2010) [9] investigated the generating process of air bubbles and their effect on seepage failure using the SPH method and model tests.

Furthermore, Fukumoto et al. (2021) [10] coupled lattice Boltzmann and distinct element methods for seepage flow and soil particle motion to perform two-dimensional direct simulations. The simulations were performed at the scale of a model experiment based on soil particles of a size equivalent to actual sand. The analysis results indicated that the typical seepage failure behaviors could be reproduced seamlessly, where boiling and heaving occurred downstream near the sheet pile and finally led to quicksand.

In conventional design methods, the soil foundation stability inside cofferdams is usually evaluated only from the balancing weight of soil material and upward seepage force. However, the mechanical properties of soil material and the scale effect of soil particles need to be sufficiently considered. In addition, whether the shape of the water channel observed during sand boiling model cofferdams help predict the real-scale scour shape is unclear. Therefore, developing models to predict the failure mode and scale is crucial to evaluate the performance of cofferdams. In particular, when numerical methods are implemented to simulate large deformation problems, these methods should be accurate as they depend on geomaterial properties. Thus, to validate the accuracy of the numerical analysis method, collecting experimental data is essential to evaluate seepage failure modes and the following erosion process associated.

In this study a series of model tests on sand boiling occurrence inside a cofferdam were conducted. In particular, two cofferdam models of different sizes were used, and the model ground was formed considering several ground materials with different grain size distributions and different relative densities. Finally, the seepage flow and ground behavior up to the onset of sand boiling were observed in all model tests.

2. RESEARCH SIGNIFICANCE

This study clarifies the differences in the seepage fracture process for the onset of sand boiling inside the cofferdam depending on the grain size and density of the geomaterials. Furthermore, the influence of the scale effect on the seepage failure phenomenon in the model experiment is clarified through experiments with different scales. This study will help to improve the accuracy of model experiments for clarifying seepage fracture phenomena.

3. MODEL TESTS

3.1 Experimental and Measurement Device

The experimental setup schematic is shown in Fig. 1. Two scales were used for the model tests. The dimensions of the apparatus are listed in Table 1. Each scale model test is referred to as a standard model test and a small model test, with the small model being 1/4 of the scale of the standard model. However, the depth of the small-model test was not 1/4 because the apparatus used in the small-model test was pre-made. Therefore, the water injection volume was adjusted to satisfy the similarity described in the next section.

The experimental apparatus was set up with a divider in the center to simulate a sheet pile in a

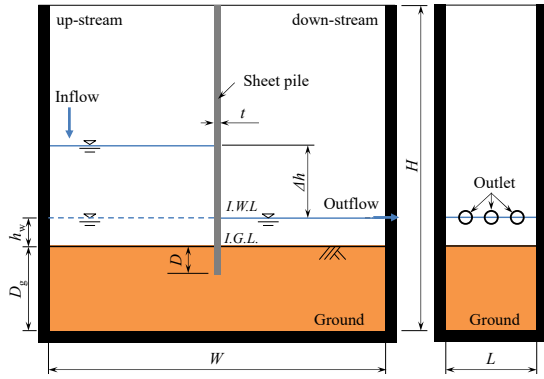


Fig. 1 Schematic of model test apparatus: (left) front view; (right) side view

Table 1 The scales of model devices

	Small scale	Standard scale
H (mm)	145	600
W (mm)	150	600
L (mm)	39	200
t (mm)	3	10
D (mm)	13	50
D_g (mm)	38	150
h_w (mm)	15	50

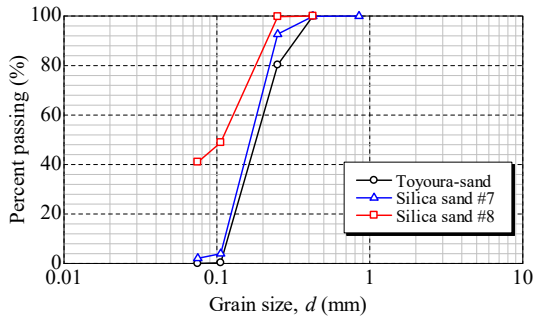


Fig. 2 Particle size distribution curve of geomaterials

Table 2 Physical properties of geomaterials

Properties	Silica #8	Silica #7	Toyouira sand
D_{50} (mm)	0.109	0.168	0.189
e_{max}	1.218	1.057	0.999
e_{min}	0.670	0.650	0.632
k_{40} (m/s)	3.02×10^{-5}	1.16×10^{-4}	1.96×10^{-4}
k_{80} (m/s)	1.41×10^{-5}	6.96×10^{-5}	1.18×10^{-4}

cofferdam. The divider was fixed to both sidewalls. Drainage outlets were placed on both sides of the

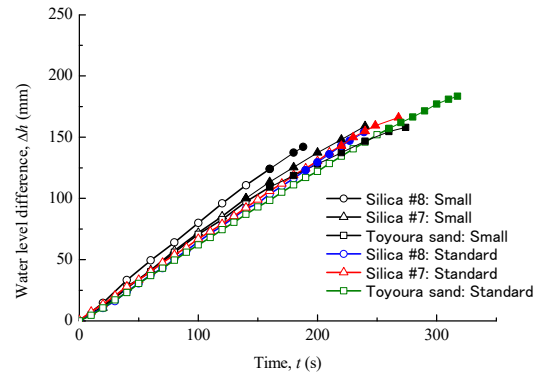


Fig. 3 Time history of water level difference at relative density $D_r = 40\%$

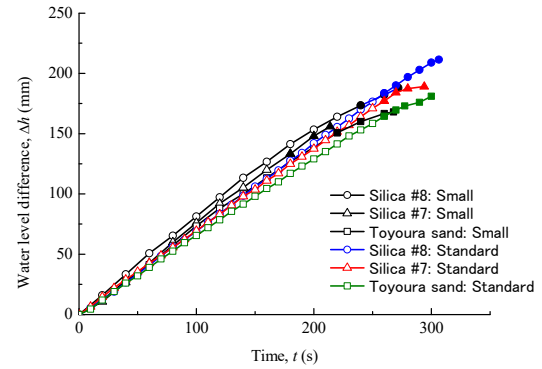


Fig. 4 Time history of water level difference at relative density $D_r = 80\%$

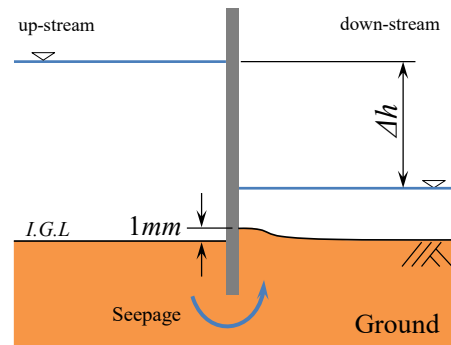


Fig. 5 Schematic diagram of the condition with displacement head difference

apparatus. During the experiment, the apparatus downstream was opened and drained to maintain a constant water level on the downstream side. In contrast, the upstream drain was closed, and a pump was used to inject water at a constant flow rate.

A high-speed camera and a video camera were used to capture the phenomena during the experiment. In addition, pore water pressure gauges were used in the standard model test to measure the

Table 3 Displacement head difference

Head difference (mm)	Displacement head difference	
	$D_r = 40\%$	$D_r = 80\%$
Silica #8	123 (120)	184 (168)
Silica #7	146 (104)	177 (140)
Toyoura sand	155 (113)	164 (146)

Table 4 Failure head difference

Head difference (mm)	Failure head difference	
	$D_r = 40\%$	$D_r = 80\%$
Silica #8	154 (143)	212 (188)
Silica #7	159 (160)	189 (156)
Toyoura sand	184 (160)	188 (170)

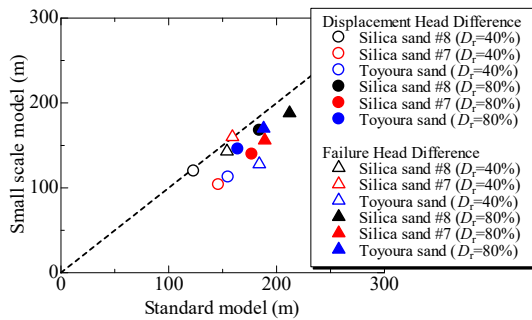


Fig. 6 Water level difference compared between standard and small scale model

change in pore water pressure at seven locations along the sheet pile perimeter.

3.2 Experimental Condition

Three geomaterials were used in the model tests: silica sand No. 8, silica sand No. 7 (hereinafter referred to as silica sand #8 and silica sand #7), and Toyoura sand. The grain size distribution of the geomaterials is shown in Fig. 2, with their main physical properties listed in Table 2. The model tests were conducted at relative densities of $D_r = 40\%$ and $D_r = 80\%$ for all sediment ground conditions to examine differences in seepage failure phenomena due to density. The properties k_{40} and k_{80} represent the permeability at 40% and 80% relative density D_r , respectively. Soil ground was deposited at a given density using the underwater drop method. For the relative density $D_r = 80\%$, the sediment ground was compacted to construct a dense ground.

Water was injected upstream by using a pump. The pump flow rates were 1.29 cm³/s and 42.9 cm³/s for the small and medium models,

Table 5 The time to reach displacement head difference

Time (s)	Displacement head difference	
	$D_r = 40\%$	$D_r = 80\%$
Silica #8	190 (153)	260 (228)
Silica #7	225 (140)	260 (184)
Toyoura sand	255 (162)	265 (212)

Table 6 The time to reach failure head difference

Time (s)	Failure head difference	
	$D_r = 40\%$	$D_r = 80\%$
Silica #8	239 (188)	307 (272)
Silica #7	268 (242)	294 (214)
Toyoura sand	318 (275)	292 (268)

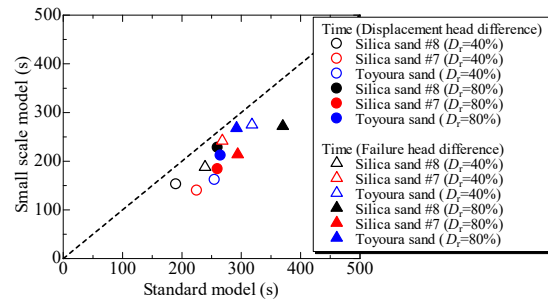


Fig. 7 Reach time for each water level difference compared between standard and small scale model

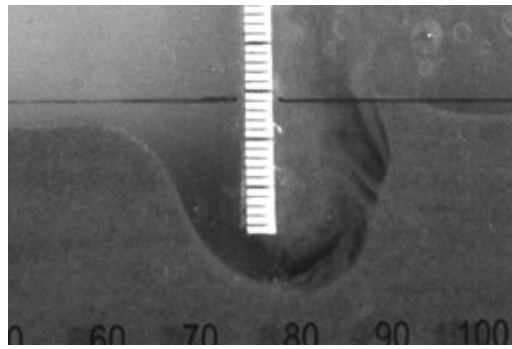
respectively, according to Froude's law.

4. EXPERIMENTAL RESULTS

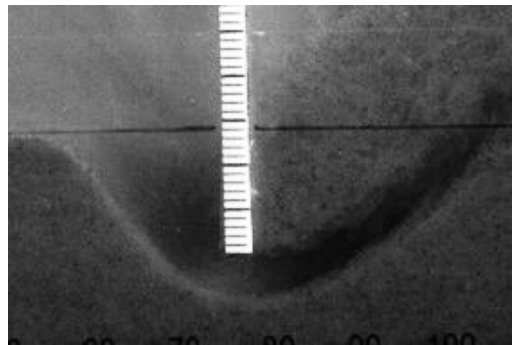
The similarities were investigated by examining the experimental data for the small model tests with the standard scale, with double time and quadruple length. In Tables 3–8, the values in parentheses indicate the experimental results for the small model and those outside the parentheses for the standard model.

4.1 Fluctuation of Hydraulic Head Difference

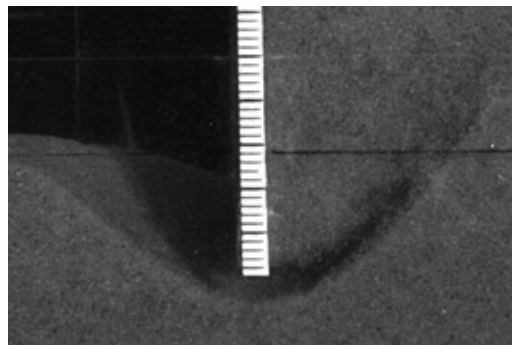
Figs. 3 and 4 show the time histories of the hydraulic head difference across the sheet pile upstream and downstream. Fig. 3 shows the relative density of $D_r = 40\%$, while Fig. 4 shows the relative density of $D_r = 80\%$. The trend of the hydraulic-head difference was similar regardless of the experimental scale, confirming that the external force conditions given by the water injection rate were similar. The trend over time indicates that the gradient changes after a certain amount of time have



(a)



(b)

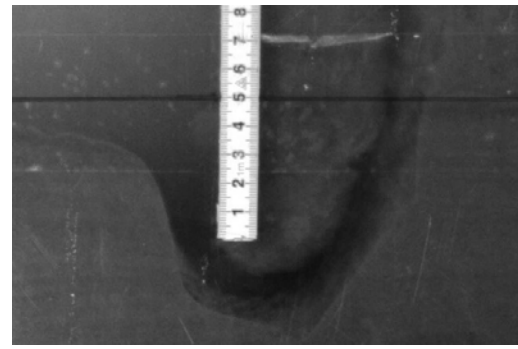


(c)

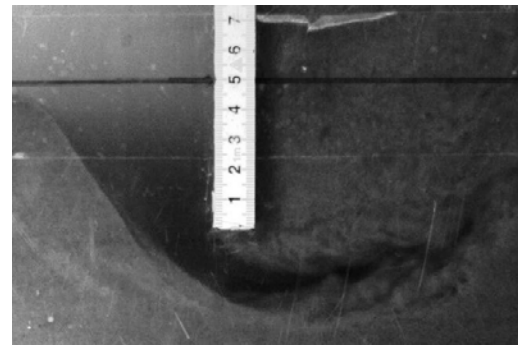
Fig. 8 Scour shape for maximum scour depth at $D_r = 40\%$ in the small-scale model: (a) Silica sand #8; (b) Silica sand #7 and (c) Toyoura sand.

elapsed since the initial gradient. The phenomena at the time of slope change were visually confirmed to indicate that deformation had occurred in the sediment.

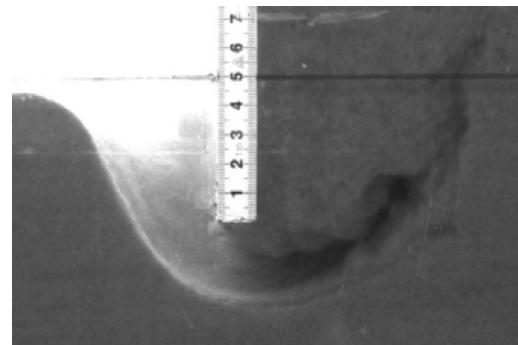
The head difference at that point is summarized in Tables 3 and 4. Moreover, the time to reach each head difference is listed in Tables 5 and 6. The time when the sediment ground downstream was uplifted by 1 mm was defined as the displacement head difference (Fig. 5), and the time when a major failure occurred was defined as the failure head difference. The values outside the parentheses in the table indicate the values obtained in the standard model test, and the values inside the parentheses are those obtained by scaling the results of the small



(a)



(b)

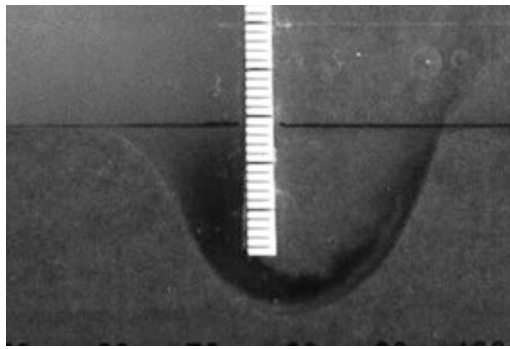


(c)

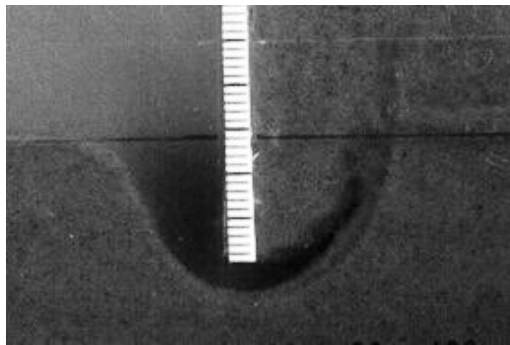
Fig. 9 Scour shape for maximum scour depth at $D_r = 40\%$ in the standard model: (a) Silica sand #8; (b) Silica sand #7 and (c) Toyoura sand.

model test to adjust them to the standard model. In Figs. 3 and 4, the markers are filled after the transformed hydraulic head difference is reached.

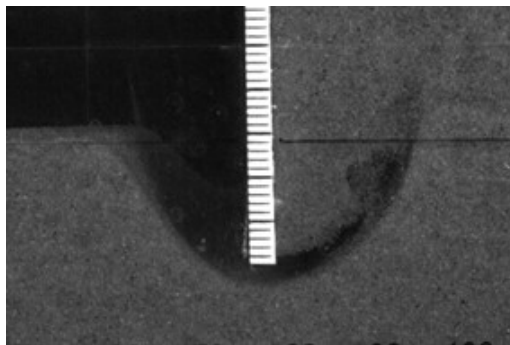
Tables 3 and 4 show that the sediment ground in the small model tends to deform at a lower hydraulic head difference than the standard model, leading to seepage failure. Regarding the relative density, for loose ground with $D_r = 40\%$ in the standard model test, the displacement and failure head differences increased as the grain size of the material increased. In contrast, for tightly packed ground with $D_r = 80\%$, each head difference increased as the grain size of the material decreased. However, the small model test did not exhibit a uniform trend or arrival time.



(a)



(b)



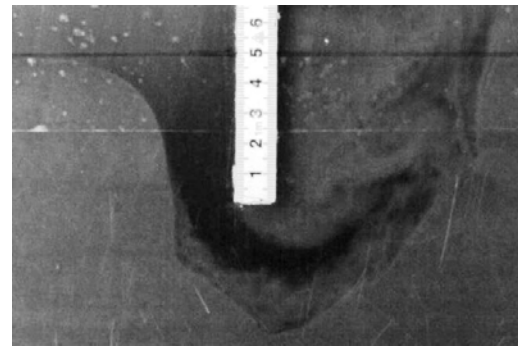
(c)

Fig. 10 Scour shape for maximum scour depth at $D_r = 40\%$ in the small-scale model: (a) Silica sand #8; (b) Silica sand #7 and (c) Toyoura sand.

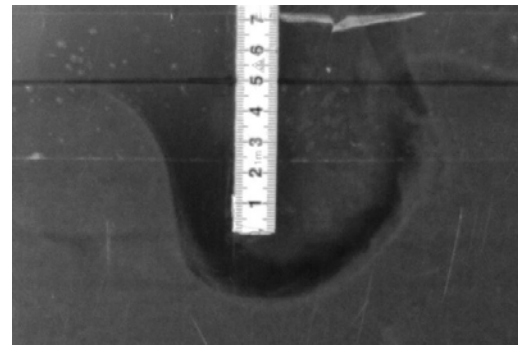
Tables 5 and 6 show that regardless of density, the sediment ground in the small model deforms and fails earlier than the sediment ground in the standard model for all geomaterials. Regarding the relative density, the arrival times of the loosely packed ground with $D_r = 40\%$ in the standard model tests increased with increasing grain size, while the arrival times of the dense ground with $D_r = 80\%$ were almost the same regardless of the material. However, no such trend was observed in the small model tests.

4.2 Scour Shape of Sediment Ground

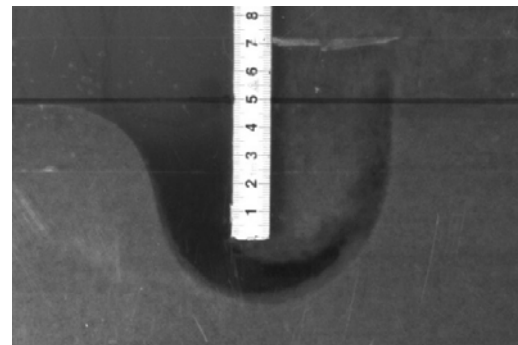
Figs. 8–11 and 12 and 13 shows the snapshots



(a)



(b)



(c)

Fig. 11 Scour shape for maximum scour depth at $D_r = 40\%$ in the standard model: (a) Silica sand #8; (b) Silica sand #7 and (c) Toyoura sand.

and plots of the scour shapes at the maximum scour depth under the sheet pile was reached for each material with a relative density of $D_r = 40\%$ and $D_r = 80\%$, respectively. The maximum scour depth was defined as the depth at which the scour depth around the sheet pile reached its maximum during the seepage failure process. In addition, the maximum scour width was defined as the horizontal distance between the upstream and downstream sides of the sheet pile. Table 5 lists the values of the maximum scour depth and width for the standard model and small model tests, respectively. Fig. 14 shows a schematic defining the maximum scour depth and width. The maximum scour width was defined as the width at the maximum scour depth.

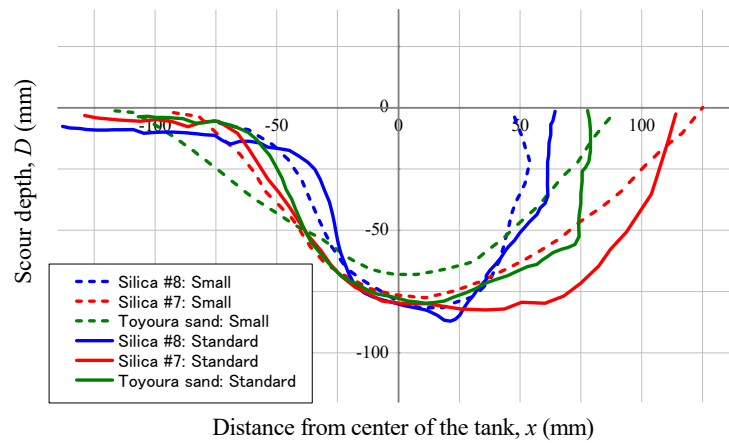


Fig. 12 Scour shape when maximum scour depth is reached at relative density $D_r = 40\%$

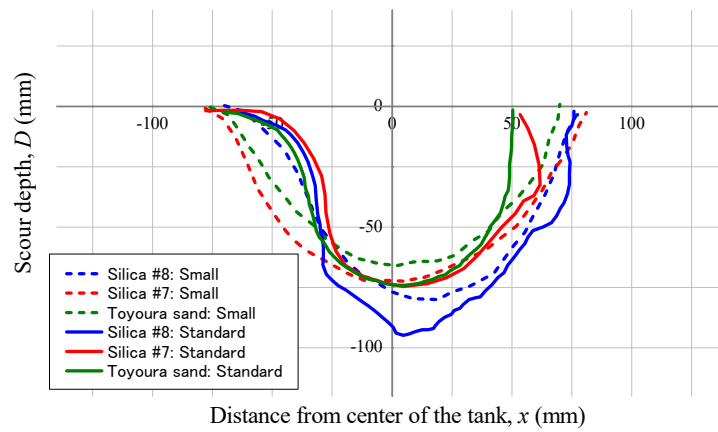


Fig. 13 Scour shape when maximum scour depth is reached at relative density $D_r = 80\%$

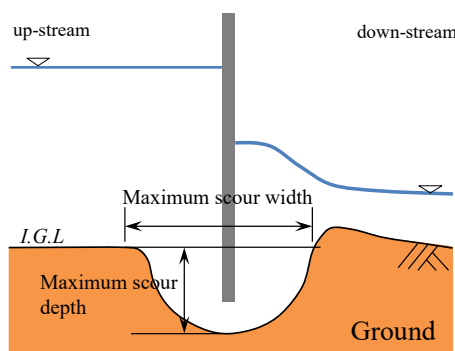


Fig. 14 Schematic diagram defining maximum scour depth and maximum scour width

The maximum scour depth of each material was similar regardless of the relative density. In contrast, the maximum scouring width varied depending on the relative density, and the loosely packed soil with a relative density of $D_r = 40\%$ tended to have a

Table 7 Maximum scour depth

(mm)	Maximum scour depth	
	$D_r = 40\%$	$D_r = 80\%$
Silica #8	87 (80)	95 (80)
Silica #7	83 (76)	75 (72)
Toyouira sand	80 (68)	74 (64)

Table 8 Maximum scour width

(mm)	Maximum scour width	
	$D_r = 40\%$	$D_r = 80\%$
Silica #8	64 (56)	76 (80)
Silica #7	114 (124)	62 (80)
Toyouira sand	79 (88)	50 (68)

wider scouring width, indicating that the scouring area was wider. In addition, the scour profile of the

loose soil with $D_r = 40\%$ differed from that of the dense soil with $D_r = 80\%$, indicating that the scour shape varied depending on the geomaterial.

Focusing on the scale effects of the model test, the results of the small model were similar to or slightly underestimated compared to those of the standard model regarding the maximum scour depth and scour shape, as indicated in Table 7. In contrast, the small model overestimated the maximum scour width compared with the standard model in Table 8.

5. CONCLUSIONS

We conducted seepage flow tests on model cofferdams to analyze seepage flow and ground deformation behaviors. Two models of cofferdams with different model scales and several ground materials with different grain size distributions and different relative densities were employed. The conclusions of this study can be summarized as follows:

- The perceptible effect of the model scale on the critical hydraulic-head difference between the inside and outside cofferdams was observed. The critical hydraulic head difference for the small-scale model was smaller than that for the standard-scaled model.
- The grain size and relative density of the ground material affected the shapes of the water channel from outside to inside the cofferdam during sand boiling. In contrast, the cofferdam model scale barely affected the shape of the channel.

6. ACKNOWLEDGMENTS

This work was supported by JSPS Grant-in-Aid for Scientific Research (C) 17K06553, JSPS Grant-in-Aid for Young Scientists 20K14824, The Geoscience Center Foundation, and Research Funding Granted by Toyohashi University of Technology President. We thank Erika Yagami, Yuki Ando, and Nur Atiqah Syazrina Binti Aziz for their help in conducting the model tests.

7. REFERENCES

[1] Terzaghi K., and Peck R. B., Soil Mechanics in Engineering Practice, John Wiley and Sons,

1948, pp. 218–233.

- [2] Miura K., Imafuku M., Furukawa N., and Nagasawa M., Ground failure due to seepage flow in a river cofferdam, *Soil mechanics and Foundation Engineering*, Vol. 47 (4), 1999, pp. 7–10. (in Japanese)
- [3] Miura K., Supachawarote C., Phien-Wej N., and Lin D. G., Boiling resistant design of cofferdams regarding the 3-D effects of seepage, *The 15th International Conference on Soil Mechanics and Geotechnical Engineering (15ISSMGE)*, 2001, pp. 2151–2154.
- [4] Tanaka T., and Verruijt A., Seepage failure of sand behind sheet piles -The mechanism and practical approach to analyze-, *Soils and Foundations*, Vol. 39, Issue 2, 1999, pp. 27–35.
- [5] Asaoka A., and Kodaka T., Seepage failure experiment and their analysis of loose and medium dense sands. *Soils and Foundations*, Vol. 32, Issue 3, 1992, pp. 117–129.
- [6] Benmebarek N., Benmebarek S., and Kastner R., Numerical studies of seepage failure of sand within a cofferdam, *Computers and Geotechnics*, Vol. 32, 2005, pp. 264–273.
- [7] Okajima K., Tanaka T., Zhang S., and Komatsu T., Model experiments and elasto-plastic finite element analysis about seepage failure of sand behind fixed sheet pile, *Transaction of the JSIDRE*, Vol. 260, 2009, pp. 107–112.
- [8] Maeda K., and Sakai M., Development of seepage failure analysis procedure of granular ground with Smoothed Particle Hydrodynamics (SPH) method, *Journal of Applied Mechanics*, JSCE, Vol. 7, 2004, pp. 775–786.
- [9] Maeda K., and Sakai M., Seepage failure and erosion of ground with air bubble dynamics, *ASCE, Geoenvironmental Engineering and Geotechnics*, 2010, pp. 261–266.
- [10] Fukumoto Y., Yang H., Hosoyamada T., and Ohtsuka S., 2-D coupled fluid-particle numerical analysis of seepage failure of saturated granular soils around an embedded sheet pile with no macroscopic assumptions, *Computers and Geotechnics*, 2021, Vol. 136, 104234.

Copyright © Int. J. of GEOMATE All rights reserved, including making copies, unless permission is obtained from the copyright proprietors.
